This paper was submitted to the Journal of Geophysical Research

(We have change a Title; former Title was "Are Ring Current Ions Lost in Dispersion Relation of Electromagnetic Ion Cyclotron Waves?")

Impact of Ring Current Ions on Electromagnetic Ion Cyclotron Wave Dispersion Relation

G. V. Khazanov

NASA, Marshall Space Flight Center, Huntsville, Alabama, USA

K. V. Gamayunov

NASA, Marshall Space Flight Center, Huntsville, Alabama, USA

Short title: RC ROLE IN EMIC WAVE DISPERSION RELATION

Abstract. Effect of the ring current ions in the real part of electromagnetic ion cyclotron wave dispersion relation is studied on global scale. Recent Cluster observations by *Engebretson et al.* [2007] showed that although the temperature anisotropy of energetic (> 10 keV) ring current protons was high during the entire 22 November 2003 perigee pass, electromagnetic ion cyclotron waves were observed only in conjunction with intensification of the ion fluxes below 1 keV by over an order of magnitude. To study the effect of the ring current ions on the wave dispersive properties and the corresponding global wave redistribution, we use a self–consistent model of interacting ring current and electromagnetic ion cyclotron waves [*Khazanov et al.,* 2006], and simulate the May 1998 storm. The main findings of our simulation can be summarized as follows: First, the plasma density enhancement in the night MLT sector during the main and recovery storm phases is mostly caused by injection of suprathermal plasma sheet H^+ ($\lesssim$ 1 keV), which dominate the thermal plasma density. Second, during the recovery storm phases, the ring current modification of the wave dispersion relation leads to a qualitative change of the wave patterns in the postmidnight–dawn sector for L > 4.75. This "new" wave activity is well organized by outward edges of dense suprathermal ring current spots, and the waves are not observed if the ring current ions are not included in the real part of dispersion relation. Third, the most intense wave–induced ring current precipitation is located in the night MLT sector and caused by modification of the wave dispersion relation. The strongest precipitating fluxes of about $8 \cdot 10^6$ $(\mathrm{cm}^2 \cdot \mathrm{s} \cdot \mathrm{sr})^{-1}$ are found near L=5.75, MLT=2 during the early recovery phase on 4 May. Finally, the nightside precipitation is more intense than the dayside fluxes, even if there are less

intense waves, because the convection field moves ring current ions into the loss cone on the nightside, but drives them out of the loss cone on the dayside. So convection and wave scattering reinforce each other in the nightside, but interfere in the dayside sector.

1. Introduction

Electromagnetic ion cyclotron (EMIC) waves are a common feature of the Earth magnetosphere. These waves were observed in the inner [e. g., *LaBelle et al.,* 1988; *Erlandson and Ukhorskiy,* 2001] and outer [*Anderson et al.,* 1992a, b] magnetosphere, at geostationary orbit [*Young et al.,* 1981; *Mauk,* 1982], at high latitudes along the plasmapause [*Erlandson et al.,* 1990], and at ionospheric altitudes [*Iyemori and Hayashi,* 1989; *Bräysy et al.,* 1998]. Interaction of the ring current (RC) with EMIC waves causes scattering of ions into the loss cone and leads to decay of the RC [*Cornwall et al.,* 1970]. This wave–induced RC precipitation was studied widely both experimentally and theoretically [e. g., *Soraas et al.,* 1999; *Erlandson and Ukhorskiy,* 2001; *Yahnina et al.,* 2003; *Walt and Voss,* 2001, 2004; *Jordanova et al.,* 2001; *Khazanov et al.,* 2002], which produce RC decay times of about one hour or less during the main phase of storms [*Gonzalez et al.,* 1989]. Obliquely propagating EMIC waves damp due to Landau resonance with thermal plasmaspheric electrons, and cyclotron resonances with thermal, suprathermal, and hot heavy ions [e. .g., *Cornwall et al.,* 1971; *Anderson and Fuselier,* 1994; *Horne and Thorne,* 1997; *Thorne and Horne,* 1994; 1997]. Subsequent transport of the dissipating wave energy into the ionosphere causes ionosphere temperature enhancements [e. g., *Gurgiolo et al.,* 2005]. *Cornwall et al.* [1971] employed the mechanism of resonant energy transfer to electrons to explain stable auroral red arc emissions during the recovery phase of storms. Measurements taken aboard the Prognoz satellites revealed a "hot zone" near the plasmapause where

the temperature of core plasma ions can reach tens of thousands of degrees [*Bezrukikh and Gringauz,* 1976; *Gringauz,* 1983; 1985]. The earliest results regarding the heating of the cold ions were obtained by *Galeev* [1975] who considered the induced scattering of EMIC waves by plasmaspheric protons as an ion heating mechanism. This nonlinear wave–particle interaction process was used in a plasmasphere–RC interaction model by *Gorbachev et al.* [1992]. Later, a detailed analysis of thermal ion heating by EMIC waves was presented by *Anderson and Fuselier* [1994] and *Fuselier and Anderson* [1996]. Relativistic electrons ($\geq$ 1 MeV) in the outer radiation belt can also interact with EMIC waves [*Thorne and Kennel,* 1971; *Lyons and Thorne,* 1972]. Recently, data from balloon–borne X–ray instruments provided indirect but strong evidence for EMIC wave–induced precipitation of outer–zone relativistic electrons [*Foat et al.,* 1998; *Lorentzen et al.,* 2000]. These observations stimulated theoretical and statistical studies [*Summers and Thorne,* 2003; *Albert,* 2003; *Meredith et al.,* 2003; *Loto'aniu et al.,* 2006] which demonstrated that EMIC wave–induced pitch–angle diffusion of MeV electrons can operate in the strong diffusion limit with a time scale of several hours to a day, and that this mechanism can compete with relativistic electron depletion caused by the adiabatic effect of *Dst* during the initial and main phases of a storm. Therefore, EMIC waves interact well with both the magnetospheric electrons and ions, and these waves are strongly influence the particle dynamics in the eV–MeV energy range.

In a number of magnetospheric regimes, a source of free energy for the excitation of EMIC waves is the temperature anisotropy ($T_\perp > T_\parallel$) of the hot H^+ distribution [*Cornwall,* 1964, 1965; *Kennel and Petschek,* 1966]. Our understanding of EMIC

wave growth and propagation was dramatically changed after measurements on board the GEOS 1 and 2 satellites. They revealed the critical role of the thermal He^+ for generation and propagation of EMIC waves [*Young et al.,* 1981; *Roux et al.,* 1982]. The observations stimulated theoretical studies in which the influence of thermal He^+ and O^+ admixtures on EMIC wave properties was considered [*Mauk,* 1982; *Roux et al.,* 1982; *Rauch and Roux,* 1982; *Gomberoff and Neira* 1983; *Gendrin et al.,* 1984; *Denton et al.,* 1992; *Horne and Thorne,* 1993]. The effects of energetic RC heavy ions (He^+ and O^+) on the generation of EMIC waves in a multi–ion core plasma (H^+, He^+, O^+) were studied by *Kozyra et al.* [1984]. *Horne and Thorne* [1993] used the "HOTRAY" ray tracing program to study the role of propagation and refraction in the generation of different branches of EMIC waves in a multi–ion thermal plasma. They found that the local growth rate alone cannot determine the resulting wave amplification; propagation effects have a major impact on the path–integrated wave gain, and consequently the prevalent He^+–mode grows preferably at the plasmapause. Recently, *Loto'aniu et al.* [2005] used magnetic and electric field data from the Combined Release and Radiation Effects Satellite to obtain the Poynting vector for Pc 1 EMIC waves. They found bidirectional wave energy propagation, both away and toward the equator, for events observed below 11° |MLAT|, but unidirectional energy propagation away from the equator for events outside ±11° of the equator. *Engebretson et al.* [2005] found a similar EMIC wave energy propagation dependence, with mixed direction within approximately ±20° MLAT, but consistently toward the ionosphere for higher magnetic latitudes. These observations allowed *Engebretson et al.* [2007] to state that "the mixed directions

observed in the above studies near the equator is evidence of wave reflection at the off–equatorial magnetic latitude corresponding to the ion–ion hybrid frequency. Waves that reflect would then set up a standing (bi–directional) pattern in the equatorial magnetosphere. Waves that tunnel through would tend to be absorbed in the ionosphere and not be able to return to equatorial latitudes."

Starting from the pioneering work of *Kennel and Petschek* [1966], it is well–known that the plasma density is one of the most important plasma characteristics controlling EMIC wave generation; the minimum energy of resonant ions is proportional to the magnetic field energy per particle. In an electron–proton plasma, *Cornwall et al.* [1970] found that the EMIC wave growth rate maximizes just inside the plasmapause where the Alfvén speed is low, falling to zero with both decreasing (because of electron–ion collisions) and increasing L–shell (because of high critical anisotropy). In the case of a multi–ion magnetosphere, *Horne and Thorne* [1993] reported a result opposite to that found by *Cornwall et al.* [1970], namely, the growth rates are substantially greater outside the plasmapause than just inside the plasmapause. The latter is an effect of heavy ions, and both the above results were reconciled by *Kozyra et al.* [1984]. However, *Horne and Thorne* [1993] illustrated that when propagation effects are properly included, the path–integrated wave gain is indeed larger just inside the plasmapause. The effect of the plasmapause in EMIC wave generation is very clearly observed both in experiments [e. g., *Fraser and Nguyen,* 2001], and in the results of numerical simulation [*Kozyra et al.,* 1997; *Khazanov et al.,* 2006]. (Of course, the real magnetospheric situation is more complex, and wave occurrence actually increases with

L–shell, which depending on MLT, exhibits a radial structure with a gap between high and low L–shell events [*Anderson et al.*, 1992a].)

Recently, *Engebretson et al.* [2007] presented the Cluster observations of EMIC waves in the Pc 1–2 frequency range and associated ion distributions during the October and November 2003 storms. The most intense waves were observed on 22 November near the end of the rapid recovery phase in the dawn MLT sector at L=4.4–4.6. Generation of these waves was associated with anisotropic RC H^+ of energies greater than 10 keV. Although the temperature anisotropy of these energetic protons was high during the entire 22 November event, EMIC waves were observed only in conjunction with intensification of the ion fluxes below 1 keV by over an order of magnitude. This suggests that a suprathermal plasma plays an important role in the destabilization of the more energetic RC and/or plasma sheet ions, because high energy anisotropic RC and/or plasma sheet proton distributions appeared to be a necessary but not sufficient condition for the occurrence of EMIC waves. Similarly, studying Pc 1–2 events in the dayside outer magnetosphere, *Engebretson et al.* [2002] and *Arnoldy et al.* [2005] found that greatly increased fluxes of low energy protons are crucial for the destabilization of the anisotropic RC protons. Those observations provide clear evidence that both the cold plasmaspheric plasma (and, of course, heavy ion content) and the suprathermal ($\lesssim$ 1 keV) ions injected from the plasma sheet (and/or ion outflow from the ionosphere) control EMIC wave excitation in the RC. On the other hand, an assumption that the total plasma density/composition is dominated by the thermal plasma was made in previous RC–EMIC wave modeling efforts, and RC ions were not included in the real

part of the wave dispersion relation [*Kozyra et al.,* 1997; *Jordanova et al.,* 1998b, 2001; *Khazanov et al.,* 2006], but only in the EMIC wave growth rate. As a result, EMIC waves are only generated near the plasmapause in all these theoretical models. Consequently we generalize our previous self–consistent RC–EMIC wave model [*Khazanov et al.,* 2006] to take into account the effect of RC ions in the real part of the EMIC wave dispersion relation.

The present study further develops a self–consistent theoretical model of RC and propagating EMIC waves in a multi–ion magnetospheric plasma [*Khazanov et al.,* 2006], where we take into account the RC ions in the real part of dispersion relation for the He^+–mode. This article is organized as follows: In section 2 we provide the system of equations which govern our global theoretical model, as well as the initial/boundary conditions used in the simulation of the May 1998 storm; In section 3 we present both the spatial distribution of the total plasma density (thermal + higher energies) during the May 1998 event, and the fine energy structure of the RC phase space distribution functions; In section 4, the effect of plasma density on the EMIC wave growth is illustrated; In section 5, role of the RC ion thermal effects in the He^+–mode dispersion relation is analyzed; In section 6, results of simulation are presented; Finally, in section 7 we summarize the new features of the model, and the findings of the paper.

2. Equations of Global Model, Approaches and Initial/Boundary Conditions

For RC species H^+, O^+, and He^+, we simulate the RC dynamics by solving the bounce–averaged kinetic equation for the phase space distribution function (PSDF), $F(r_0, \varphi, E, \mu_0, t)$. The PSDF depends on the radial distance in the magnetic equatorial plane r_0, geomagnetic east longitude φ, kinetic energy E, cosine of the equatorial pitch angle μ_0, and time t [see, e. g., *Fok et al.,* 1993; *Jordanova et al.,* 1996]. We use the bounce–averaged kinetic equation for the He^+–mode of EMIC waves to describe the wave power spectral density. This equation was originally derived by *Khazanov et al.* [2006], and explicitly includes the EMIC wave propagation, refraction and reflection in a multi–ion magnetospheric plasma. Following to *Khazanov et al.* [2006], we ignore the slow azimuthal and radial drifts of the waves during propagation, and use the reduced wave kinetic equation. So the resulting system of governing equations take the form:

$$\frac{\partial F}{\partial t} + \frac{1}{r_0^2}\frac{\partial}{\partial r_0}\left(r_0^2\left\langle\frac{dr_0}{dt}\right\rangle F\right) + \frac{\partial}{\partial \varphi}\left(\left\langle\frac{d\varphi}{dt}\right\rangle F\right) + \frac{1}{\sqrt{E}}\frac{\partial}{\partial E}\left(\sqrt{E}\left\langle\frac{dE}{dt}\right\rangle F\right) + \frac{1}{\mu_0 h(\mu_0)}\frac{\partial}{\partial \mu_0}\left(\mu_0 h(\mu_0)\left\langle\frac{d\mu_0}{dt}\right\rangle F\right) = \left\langle\left(\frac{\delta F}{\delta t}\right)_{loss}\right\rangle, \quad (1)$$

$$\frac{\partial B_w^2(r_0, \varphi, t, \omega, \theta_0)}{\partial t} + \langle\dot{\theta}_0\rangle \cdot \frac{\partial B_w^2}{\partial \theta_0} = 2\langle\gamma(r_0, \varphi, t, \omega, \theta_0)\rangle \cdot B_w^2. \quad (2)$$

In the left–hand side of equation (1), all the bounce–averaged drift velocities are denoted as $\langle\cdots\rangle$, and may be found in previous studies [*Jordanova et al.,* 1994; *Khazanov et al.,* 2003]. In equation (2), ω and θ_0 are the wave frequency and equatorial wave normal angle, respectively, $\langle\dot{\theta}_0\rangle$ is the bounce–averaged drift velocity of the equatorial wave

normal angle, B_w is the EMIC wave magnetic field, and $\langle\gamma\rangle$ is a result of averaging of the local growth/damping rates, which includes both the wave energy source due to interaction with RC ions and the energy sink due to absorption by thermal and hot plasmas, along the ray phase trajectory over the wave bounce period. Note that equation (2) is accompanied by a system of the ray tracing equations which are not written here (for details see *Khazanov et al.* [2006] and references therein).

The term in the right–hand side of equation (1) includes losses from charge exchange, Coulomb collisions, ion–wave scattering, and precipitation at low altitudes [*Jordanova et al.,* 1996, 1997; *Khazanov et al.,* 2002, 2003]. Loss through the dayside magnetopause is taken into account allowing a free outflow of the RC ions from a simulation domain. The bounce–averaged pitch angle diffusion term in the right–hand side of equation (1) is a functional of the EMIC wave power spectral density, B_w^2, i. e. the diffusion coefficient has the form $\langle D_{\mu_0,\mu_0}\rangle = \langle D_{\mu_0,\mu_0}(B_w^2(\cdot))\rangle$. On the other hand, $\langle\gamma\rangle$ in equation (2) is a functional of the phase space distribution function, F, i. e. $\langle\gamma\rangle = \langle\gamma(F(\cdot))\rangle$. So equations (1) and (2) self–consistently describes the interacting RC and EMIC waves in a quasilinear approximation. It should be emphasized that in order to describe the wave–particle interaction in equation (1) we have to know the off–equatorial power spectral density distribution for EMIC waves, and this distribution can then be mapped from the magnetic equator using solutions of the ray tracing equations.

The geomagnetic field in our simulation is taken to be a dipole field. The electric field is expressed as the shielded (exponent 2) Volland–Stern convection field [*Volland,*

1973; *Stern,* 1975] which is *Kp*–dependent, with a corotation field [see, e. g., *Lyons and Williams,* 1984]. The equatorial thermal electron density distribution is calculated with the time–dependent model of *Rasmussen et al.* [1993]. For modeling the RC–EMIC wave interaction and wave propagation we also need to know the density distribution in the meridional plane. In the present study we employ an analytical density model which includes the product of three terms; (1) diffusive equilibrium model term [*Angerami and Thomas,* 1964], (2) lower ionosphere term, and (3) plasmapause and outer magnetosphere term. This analytical model is adjusted to the *Rasmussen* model at the equator. So the resulting plasmaspheric density model provides a 3D spatial distribution for electrons, and an ion content assumed to be 77% for H^+, 20% for He^+, and 3% for O^+. Geocoronal neutral hydrogen number density, needed to calculate loss due to charge exchange, is obtained from the spherically symmetric model of *Chamberlain* [1963] with its parameters given by *Rairden et al.* [1986].

In order to study *Dst* variation during the May 1998 storm period, and to calculate the energy content for the major RC ion species, H^+, O^+, He^+, *Farrugia et al.* [2003] used the RC kinetic model of *Jordanova et al.* [1998a]. They found that during this storm the energy density of H^+ is greater than twice that of O^+ at all MLTs, and the contribution of He^+ to the RC energy content is negligible. This implies that RC O^+ content do not exceed 30% during the main phase of this storm. Note that above estimation was obtained from a simulation without oxygen band waves. On the other hand, *Bräysy et al.* [1998] observed very asymmetric O^+ RC during the main phase of the April 2–8, 1993 storm, which suggests that the RC oxygen ion loss rate is

214 considerably faster than the drift speed. This result is difficult to explain in terms of
215 charge exchange and Coulomb scattering, and suggests that the production of EMIC
216 waves contributes significantly to RC O^+ decay during the main and early recovery
217 phases. In other words, due to generation of the O^+–mode EMIC waves, most RC O^+
218 precipitates before reaching the dusk MLT sector [*Bräysy et al.,* 1998]. Therefore, to
219 estimate the RC O^+ content correctly, the O^+–mode should be included in simulation,
220 and it is likely that *Farrugia et al.* [2003] overestimated the RC O^+ content during
221 May 1998. Anyhow, the calculations of *Thorne and Horne* [1997] clearly confirm that
222 the above RC O^+ percentage cannot significantly suppress He^+–mode amplification,
223 and only slightly influences the resulting wave growth. It is for this reason we chose to
224 initially exclude RC O^+ in our particular simulation of May 2–7, 1998, and to assume
225 that the RC is entirely made up of energetic protons.

226 The night–side boundary condition is imposed at the geostationary distance in
227 our model, and we use the flux measurements during the modeled event obtained from
228 the Magnetospheric Plasma Analyzer and the Synchronous Orbit Particle Analyzer
229 instruments on the geosynchronous LANL satellites. Then, according to *Young et al.*
230 [1982], we divide the total flux measured at geostationary orbit between the RC H^+,
231 O^+, and He^+ depending on geomagnetic and solar activity as measured by Kp and $F_{10.7}$
232 indices. Only the H^+ fluxes were used as a boundary condition in the simulation.

233 To obtain the self–consistent initial conditions for equations (1) and (2), the
234 simulation was started at 0000 UT on 1 May, 1998 using a background noise level for
235 the He^+–mode of EMIC waves [e. g., *Akhiezer et al.,* 1975b], the statistically derived

quiet time RC proton energy distribution of *Sheldon and Hamilton* [1993], and the initial pitch angle characteristics of *Garcia and Spjeldvik* [1985]. The initial the RC and EMIC wave distributions are derived independently, and of course, have nothing to do with a particular state of the magnetosphere during a simulated event. Only the boundary conditions provided by the LANL satellites can be considered as data reflecting a particular geomagnetic situation (and, to a certain extent, the employed plasmasphere and electric field models driven by Kp). Therefore, before simulation of a particular geomagnetic event can be possible, we first seek an initial state for the RC and EMIC waves that is self–consistent and reflects the particular geomagnetic situation. In our case, this was done by running the model code for 24 hours. In about 20 hours of evolution, the wave magnetic energy distribution reaches a quasistationary state indicating that the RC–EMIC wave system achieves a quasi–self–consistent state. (Note that 20 hours has nothing to do with the typical time for wave amplification and instead reflects the minimum time needed to adjust RC and waves to each other and to the real prehistory of a storm.) So the self–consistent modeling of the May 1998 storm period is started at 0000 UT on 2 May (24 hours after 1 May 0000 UT) using solutions of equations (1) and (2) at 2400 UT on 1 May as the initial conditions for further simulation.

3. Distribution of Plasma Density and Energy Structure of RC PSDFs

3.1. Spatial Patterns of Plasma Density During the May 1998 Storm

From the results of our simulation we select seven snapshots which represent the intervals of the most enhanced plasma sheet H^+ injection into the RC region. The selected equatorial plasma density distributions are presented in Figure 1. The first row in this Figure shows the electron plasma density distribution from the *Rasmussen et al.* [1993] model, and the second row provides a sum of the corresponding plasma density from the first row and the RC H^+ density. Note that starting from high L–shell, the RC ions dominate the thermal plasma excepting a plasmaspheric drainage plume, and below we shell concentrate only on cases of pronounced density enhancement during plasma sheet ion injections. The first plasma sheet ion injection appears about 32 hours after 1 May, 0000 UT (not shown), which affects the density distribution for about 16 hours, while the RC ions only slightly modify the plasma density distribution after 48 hours (not shown). During this interval, the RC H^+ density dominates the thermal plasma in the dusk–midnight MLT sector (see hours 33 and 34 in Figure 1). The second ion injection starts about 56 hours (not shown). The snapshots at hour 60 show the most distinct pattern of the cold and total plasma density during this injection event when the RC H^+ dominates the thermal plasma density in the nightside through the entire dusk–dawn MLT sector. Again, there are only minor differences between the density snapshots at 68 hours (not shown). The third plasma sheet ion injection shown in

Figure 1

Figure 1 starts at about 76 hours and impacts the plasma density distribution through hour 90 (not shown). This injection is most intense comparing to previous ones, and the RC H^+ dominance is observed in the greatest L–shell and MLT extents encircling a great part of the globe during the third injection. The results of our simulation are in qualitative agreement with the RC density distribution obtained by *Zaharia et al.* [2006] during the moderate geomagnetic storm of 21–23 April 2001.

We presented only the RC H^+ density distribution above, and did not say anything about the distribution of the electron density. It is obvious that in all "slow" magnetospheric processes the quasi–neutrality condition should hold. This implies that electrons have the same density distribution as the ions. Quasi–neutrality can be sustained by both the energetic plasma sheet electrons injected along with ions, and/or the cold ionospheric electrons due to field–aligned currents. The resulting electron temperature strongly affects the Coulomb energy degradation of the RC ions, the resonant Landau damping of EMIC waves, and barely influences the EMIC wave dispersive properties (see, e. g., *Khazanov et al.* [2007], *Akhiezer et al.* [1975a]). *Khazanov et al.* [2007] demonstrated that both the EMIC wave Landau damping and collisional RC energy dissipation are maximized for an electron temperature about 1 eV. This is the temperature adopted in our RC–EMIC wave model for thermal plasma [*Khazanov et al.,* 2003]. Therefore, if we do not track the electron dynamics and keep $T_e = 1$ eV for the entire simulation domain, we can potentially underestimate the EMIC wave energy, especially at high L–shells during the main and recovery storm phases when RC ions dominate the thermal plasma. Below we assume that plasma is quasi–neutral

297 and that the electron temperature is 1 eV throughout the entire simulation domain
298 during the May 1998 event.

299 3.2. Fine Energy Structure of RC PSDFs

300 The new RC ions, injected from the plasma sheet in the night MLT sector, cause
301 impressive plasma density enhancement for high L–shells during the main and recovery
302 storm phases. This feature is clearly observed in our simulation, but in Figure 1 we
303 presented only the RC H^+ density distribution, and did not analyze the fine PSDF
304 energy structure. To consider the energy distributions of the RC H^+, we selected four
305 representative cases among the snapshots in Figure 1. The corresponding PSDFs are
306 shown in Figure 2. All the PSDFs are taken in the equatorial plane, and integrated over
307 the entire solid angle, while the effective RC proton temperature parallel to geomagnetic
308 field line, $T_{\|}$, is calculated for the entire energy range (100 eV – 430 keV). In order to
309 more clearly demonstrate change in the PSDF slope, we use a linear energy scale in a
310 low energy domain of the distribution, whereas the high energy part is depicted with
311 a logarithmic energy scale. As follows from the left–hand side of Figure 2, there is a
312 transition region in all the PSDFs which separates relatively warm ions from the more
313 hot and tenuous component. (The transition from a steep profile to more horizontal
314 profile corresponds to the transition from a small to a higher effective ion temperature.)
315 So we observe at least two ion populations which constitute the plotted RC ion PSDFs;
316 (1) the dense and relatively cold low energy RC component, and (2) the rare and
317 hotter high energy RC component. The boundary between these two ion components

is located at slightly different energy depending on each case, which from Figure 2, is about $1 - 1.5$ keV. Note that PSDFs at hours 80 and 82 include, respectively, four and three ion populations with different effective temperatures; the PSDF taken at hour 80 changes slope at energies near 1, 10, and 130 keV, whereas the PSDF at hour 82 changes slope near 0.5 and 20 keV. So the results in Figure 2 clearly demonstrate that plasma density modification due to the plasma sheet H^+ injection into the RC region is mostly caused by low energy ions with energy $\lesssim 1$ keV.

4. Effect of Plasma Density on EMIC Wave Growth

The effective proton temperatures transverse to $T_\perp$, and along $T_\parallel$, the geomagnetic field line, comply with the inequality $T_\perp > T_\parallel$ in many space plasma regimes. If the ion temperature anisotropy, $A = T_\perp/T_\parallel - 1$, exceeds some positive threshold, EMIC waves can be unstable [*Kennel and Petschek,* 1966; *Cornwall et al.*, 1970]. The growth rate for these waves critically depends on the characteristic energy for cyclotron interaction, which, as defined by *Kennel and Petschek* [1966], is just the local geomagnetic field energy per particle, having the form $E_c = B^2/(8\pi n_e)$. So, according to *Kennel and Petschek* [1966], the local growth rate for EMIC waves should be particularly sensitive to the local plasma density. Assuming that the RC is entirely made up of energetic H^+, Figure 3 plots the dependence on plasma density of the local equatorial growth/damping rate for the He^+–mode EMIC waves. Note that the calculated growth/damping rates in Figure 3 are due to the RC–wave interaction only, and the wave absorption due to thermal plasma is omitted (but, of course, this effect is included in global simulation).

All the results in Figure 3 are obtained for the wave frequency $\nu = 0.475$ Hz, and case (a) is just taken from our global model without any modification at location L=5.25, MLT=15 at 48 hours ($n_e = n_0 = 68.3$ cm^{-3}, and $B = 215.3$ nT). In order to produce the results (b), (c), and (d), we need only re–normalize the local plasma density as $n_e = 1.2 \times n_0$, $n_e = 1.5 \times n_0$, and $n_e = 2.0 \times n_0$, respectively. As follows from Figure 3, transitioning from case (a) to case (b) increases the peak growth rate by a factor 1.4, extends the region of growth, and makes the wave damping negligible. Further increase of the number density eliminates the region of wave damping. According to [*Kennel and Petschek,* 1966], the growth rate dependence on plasma density is $\gamma \sim \exp(-1/n_e)/\sqrt{n_e}$. So, although the characteristic energy decreases with increasing plasma density, the growth rate can both increase or decrease depending on the wave normal angle (see Figure 3). For a particular wave normal angle, it depends on whether we move to the growth rate maximum with density increase or whether we move from the maximum.

5. Effects of RC Temperature on EMIC Wave He^+–Mode

Although the results presented in subsection 3.2 clearly demonstrate that the observed plasma density enhancement is caused by a low energy ($\lesssim 1$ keV) population of the RC, this does not allow us to evaluate the effects of the RC ion temperature on the EMIC wave dispersive properties. In order to characterize the temperature effects in the EMIC wave dispersion relation, we use the following parameters [see, e. g., *Stix,*

1992; *Akhiezer et al.*, 1975a]

$$\lambda_i = \left(\frac{k_\perp v_{\perp,i}}{\sqrt{2}\Omega_i}\right)^2, \ \zeta_i = \left(\frac{\omega \pm \Omega_i}{k_\parallel v_{\parallel,i}}\right)^2, \ i = e, H^+, He^+, O^+, \tag{3}$$

where Ω_i is the particle gyrofrequency, and $k_\perp$ ($v_{\perp,i} = \sqrt{2T_{\perp,i}/m_i}$) and $k_\parallel$ ($v_{\parallel,i} = \sqrt{2T_{\parallel,i}/m_i}$) are the components of the wave normal vector (thermal velocity) transverse to and along geomagnetic field lines, respectively; λ_i is the squared ratio of Larmor radius to transverse wave length; and ζ_i is the squared ratio of longitudinal wave length to a typical particle displacement along the field line during a wave period. The finite Larmor radius effects are negligible if $\lambda_i << 1$. On the other hand, the plasma particles become unmagnetized if $\lambda_i >> 1$, and as a consequence the external magnetic field disappears in the wave dispersion relation. So the Larmor radius effects are most important for an intermediate case when the wave and particle parameters give $\lambda_i \sim 1$. The magnitude of ζ_i not only characterizes the importance of "longitudinal" thermal effects, but also determines the effectiveness of the resonant wave damping/growth. For instance, the number of resonating particles is small if $\zeta_i >> 1$, and as a result, plasma waves can exist for a long time without substantial damping. So the role of thermal effects in the wave dispersion relation depends on the magnitude of both ζ_i and λ_i. For example, if these parameters comply with the inequalities $\lambda_i << 1$ and $\zeta_i >> 1$, in many cases (but not always!) the leading term in a real part of dispersion relation still comes from a cold plasma approximation (limit $\lambda_i = 0$ and $\zeta_i \to \infty$, e. g., *Stix* [1992]). So depending on the magnitudes of ζ_i and λ_i, the thermal terms may be a minor correction only, or they can dominate the "cold plasma limit" term.

Until now, we discussed only the RC H^+. Although the RC H^+ dominate both O^+ and He^+ during the May 1998 storm [*Farrugia et al.,* 2003], and we do not simulate the RC O^+ and He^+ in the present study, the heavy ions participate in the RC dynamics and can influence the magnetospheric heavy ion content, especially during the main and early recovery storm phases. Despite the importance of the hot heavy ions for the EMIC wave characteristics (see, e. g., *Kozyra et al.* [1984]), in all previous studies we assumed that the total ion composition is dominated by the ion composition of the thermal plasma and did not take into account the RC ions in the real part of the wave dispersion relation [*Khazanov et al.,* 2002, 2003, 2006, 2007], including the RC ions in the imaginary part only. In all those papers, when we described the EMIC wave dispersive properties we used the electron density distribution from the time–dependent *Rasmussen et al.* [1993] model, and the ion content was assumed to be 77% for H^+, 20% for He^+, and 3% for O^+. (Although the assumed ion content is in the range of $10-30\%$ for He^+ and $1-5\%$ for O^+ following observations by *Young et al.* [1983, 1977] and *Horwitz et al.* [1981], it only approximately describes the real ion percentage and, of course, does not reflect its variability, especially during the magnetically active periods.) Now we are going to take into account the RC ions in the real part of the EMIC wave dispersion relation which can strongly modify the heavy ion percentage. In spite of this, for the purpose of comparison with previous results, we keep the earlier adopted ion percentage (77% for H^+, 20% for He^+, and 3% for O^+) throughout the entire simulation domain even if this percentage is mainly determined by the suprathermal/hot ion composition.

It follows from equation (3), assuming that all the RC ions (H^+, He^+, O^+) have

nearly the same temperature, that parameters λ_i relate to each other as masses of the corresponding RC ions. Then, considering the most dense suprathermal spots in Figure 1, we find that for the He^+–mode the following inequality

$$\lambda_{H^+} < \lambda_{He^+} < \lambda_{O^+} << 1 << \zeta_{He^+} \lesssim \zeta_{O^+} << \zeta_{H^+} \tag{4}$$

holds. Note that in order to obtain inequalities (4), we used $v_{\perp,i}$ and $v_{\parallel,i}$ calculated for the entire energy range; parameters λ_i and ζ_i could be even closer to the cold plasma limit if all the effective temperatures are calculated for a low energy RC component only (see subsection 3.2), which gives the greatest contribution to the plasma density enhancement observed in night side during the main and recovery storm phases. In the limit (4), the structure of thermal terms in the EMIC wave dispersion equation can be found, e. g., in [*Stix,* 1992; *Akhiezer et al.,* 1975a] where the finite Larmor radius effects may be omitted. The greatest thermal term ($\Lambda_\parallel$) in the dispersion equation for the EMIC wave He^+–mode comes from the RC H^+ during the May 1998 storm with the following ranking

$$\Lambda_\parallel(H^+) >> \Lambda_\parallel(O^+) \sim \Lambda_\parallel(He^+). \tag{5}$$

So only term $\Lambda_\parallel(H^+)$ can potentially compete with the "cold plasma limit" term in the He^+–mode dispersion equation. Considering the most dense suprathermal spots in Figure 1, we find that $\Lambda_\parallel(H^+)$, as a rule, can be neglected in comparison with the "cold" term in the He^+–mode dispersion relation.

6. Results and Discussions

Summarizing all the assumptions and conclusions we did in sections 3 and 5: (1) Plasma is quasi–neutral (see subsection 3.1); (2) the electron temperature is 1 eV through the entire simulation domain (subsection 3.1); (3) the plasma density enhancement observed in Figure 1 is caused by a low energy ($\lesssim$ 1 keV) population of the RC ions (subsection 3.2), while the RC H^+ ions dominate both the RC O^+ and He^+ during May 1998; (4) the ion percentage is 77% for H^+, 20% for He^+, and 3% for O^+ through the entire simulation domain (section 5); and (5) the thermal effects of electrons and the RC ions may be neglected in the real part of the He^+–mode dispersion relation (see subsections 3.1 and section 5).

6.1. Global Distribution of He^+–Mode

The equatorial (MLT, L–shell) distributions of the squared wave magnetic field,

$$B_{\mathrm{w}}^2\left(r_0,\varphi,t\right)=\int_{\omega_{min}}^{\omega_{max}}\mathrm{d}\omega\int_0^{\pi}\mathrm{d}\theta_0 B_{\mathrm{w}}^2\left(r_0,\varphi,t,\omega,\theta_0\right), \tag{6}$$

are shown in Figure 4 for the He^+–mode of EMIC waves. These simulation results Figure 4
are based on the system of governing equations (1) and (2) along with the ray tracing equations. The results in the first row are obtained when the RC ions are only treated as a source of free energy to generate EMIC waves, and omitted in the real part of the wave dispersion relation. The second row shows the case when the RC ions are taken into account in both the real and imaginary parts of the wave dispersion relation. There is an essential difference between the EMIC wave energy distributions in the first and

second rows. Modification of the EMIC wave dispersive properties due to RC ions leads to a relatively minor spatial redistribution of the "old" wave active zones presented in the first row, and mainly alters the wave intensities. The qualitative difference between the first and second rows appears during the recovery phase in the postmidnight–dawn MLT sector for L > 4.75 (hours 82 and 84). In these regions, "new" EMIC waves are generated due to modification of the wave dispersion by RC, and we do not observe any wave activity in corresponding snapshots in the first row. The B–field distributions are organized by the locations of sharp gradient in the total density of thermal plasma and RC as expected from previous studies [*Horne and Thorne,* 1993; *Khazanov et al.,* 2006]. (The sharp density drop counteracts the refraction caused by the magnetic field gradient and curvature. As a result, net refraction is suppressed, and the He^+–mode grows preferentially at these locations.) At the same time, we note that a radial extension of wave zones in the second row is slightly greater than that in the first row.

Let us now discuss the new feature caused by the modified EMIC wave dispersion and clearly observed in Figure 4. Recently, *Engebretson et al.* [2007] presented measurements of EMIC waves in the Pc 1–2 frequency range and the associated ion distributions obtained Cluster. During the October and November 2003 magnetic storms, the most intense waves were observed on 22 November near the end of a rapid recovery phase from 0825 to 0850 UT; located near dawn for L=4.4–4.6 and at an average MLAT $\approx 18°$. The waves were primarily transverse, propagated away from the equator, and predominantly left–hand polarized. Compared to the local proton gyrofrequency, these waves had a normalized frequency of X=0.34, somewhat higher

than the local He^+ gyrofrequency (X=0.25). The free energy to generate those waves was associated with anisotropic RC H^+ of energies greater than 10 keV. Note that the upper energy range of increased energy fluxes may well extend beyond the 40 keV limit of the Cluster CIS instrument. Although the temperature anisotropy of these energetic (> 10 keV) protons was high during the entire 22 November pass, EMIC waves were observed only in conjunction with intensification of the ion fluxes below 1 keV by over an order of magnitude. This suggests that the suprathermal plasma plays an important role in the destabilization of the more energetic RC and/or plasma sheet ions, and the high energy anisotropic RC and/or plasma sheet proton distributions appeared to be a necessary but not sufficient condition for the occurrence of EMIC waves. Similarly, studying Pc 1–2 events on the dayside outer magnetosphere, *Engebretson et al.* [2002] and *Arnoldy et al.* [2005] found that greatly increased fluxes of low energy protons are crucial for the destabilization of the high energy anisotropic RC protons.

The satellite observations by *Engebretson et al.* [2007] support our theoretical results presented in Figure 4. Indeed, in the second row we see intense EMIC waves (up to a few nT^2) in the postmidnight–dawn sector (for $L > 4.75$) during the recovery phase from 82 to 84 hours. This wave activity is not observed if the RC ions are not included in the real part of the wave dispersion relation (compare the first and second rows in Figure 4). At the same time, we note that *Engebretson et al.* [2007] observed waves with a normalized frequency X=0.34, whereas we consider the He^+–mode of EMIC waves with $X < 0.25$. (The most intense burst of Pc 1 waves studied by *Arnoldy et al.* [2005] was measured by the Polar satellite with a local normalized frequency of X=0.2, so the

459 waves were also He^+–mode.) For the purpose of comparison with previous results, in
460 the present study we kept the ion percentage the same as in our earlier studies, namely,
461 77% for H^+, 20% for He^+, and 3% for O^+. Then the most effective generation takes
462 place for the He^+–mode in the frequency range $\Omega_{O^+} < \omega < \Omega_{He^+}$ [see, e. g., *Kozyra et*
463 *al.,* 1984; *Horne and Thorne,* 1993; *Khazanov et al.,* 2003]. (Note that only waves in
464 the left–hand polarized part of the dispersive surface can grow, and the corresponding
465 wave frequencies should be in the range between the cross–over frequency and Ω_{He^+}.)
466 This heavy ion content, however, differs strongly from the ion percentage reported by
467 *Engebretson et al.* [2007]. For example, they observed 81% of H^+, 3% of He^+, and 16%
468 of O^+ on November 22, 2003 at 0740 UT, qualitatively different from the percentage
469 we used in the simulation. Such a great amount of RC O^+, in combination with small
470 amounts of He^+, should suppress the He^+–mode, and conversely favor the H^+–mode.
471 Self–consistent modeling of the H^+–mode is beyond the scope of the current study, and
472 should be done separately. (Strictly speaking, EMIC waves are very sensitive to the
473 the heavy ions, so wave simulation requires more realistic dynamic models of the global
474 distribution for each ion species which, unfortunately, are currently not available.) At
475 present, we believe that the crucial role of low energy RC and/or plasma sheet protons
476 in the destabilization of the high energy anisotropic RC protons is well established both
477 experimentally and theoretically. We also think that this feature depends on the wave
478 mode only quantitatively, and the qualitative effect itself does not depend on the wave
479 mode.

480 ## 6.2. Wave–Induced RC Precipitation

One of the most pronounced consequences of the RC–EMIC wave interaction is the scattering of RC ions into the loss cone. This process is one of the processes that lead to decay of RC [see, e. g., *Cornwall et al.,* 1970], especially during the main and early recovery phases of storms when decay time of about one hour or less is possible [*Gonzalez et al.,* 1989]. The EMIC wave–induced RC precipitation was studied widely both experimentally and theoretically [e. g., *Erlandson and Ukhorskiy,* 2001; *Yahnina et al.,* 2003; *Walt and Voss,* 2001, 2004; *Jordanova et al.,* 2001]. Although the effect of EMIC waves on RC ion precipitation during the May 1998 storm was discussed previously [e. g., *Khazanov et al.,* 2002, 2007], we present a few precipitating patterns that demonstrate the new features caused by modification of the EMIC wave dispersion relation. The RC precipitating flux is calculated as

$$J_{lc} = \frac{1}{\Omega_{lc}} \int_{E_1}^{E_2} \mathrm{d}E \int_{\mu_{lc}}^{1} \mathrm{d}\mu_0 j, \; \Omega_{lc} = \int_{\mu_{lc}}^{1} \mathrm{d}\mu_0, \tag{7}$$

481 where μ_{lc} is the cosine of the equatorial pitch angle at the boundary of loss cone, and
482 j is the equatorial ion differential flux. In Figure 5 we show selected snapshots of the Figure 5
483 precipitating fluxes integrated over the energy range $1 - 50$ keV. As before, the first
484 row shows the results without the RC ions in the real part of the EMIC wave dispersion
485 relation, while the second row shows precipitation when the RC ions are taken into
486 account in both the real and imaginary parts of the wave dispersion relation. There are
487 many differences between the first and second rows. The most intense ion precipitation
488 is due to "new" wave activity, and located in the night MLT sector. The strongest

fluxes of about $8 \cdot 10^6$ $(\mathrm{cm}^2 \cdot \mathrm{s} \cdot \mathrm{sr})^{-1}$ are observed near L=5.75, MLT=2 during the early recovery phase of the storm (see hour 82 in Figure 5). This precipitation is two times greater than a greatest flux from a previous study of the May 1998 storm by *Khazanov et al.* [2007]. The very interesting result can be derived by comparing Figure 5 with Figure 4; the wave–induced night side precipitation is more intense than the day side fluxes, even if there are less intense waves (compare locations L=4.5, MLT=16, and L=5.75, MLT=2 in the 82 hour snapshots). The major reason for this feature is a magnetospheric convection field which acts oppositely in day and in night sides moving RC ions into the loss cone on the nightside, and driving them out of the loss cone on the dayside. So the magnetospheric convection and the wave scattering reinforce each other on the nightside, but subtract on the dayside. Of course, we have to recall that characteristics of the wave normal angle distribution can strongly impact the effectiveness of RC ion scattering [*Khazanov et al.,* 2007].

7. Conclusions

In this paper we have further developed a self–consistent model of RC ions and propagating EMIC waves by *Khazanov et al.* [2006]. We have taken into account RC ions in the real part of dispersion relation for the He^+–mode of EMIC waves. This is a new feature of the present model and generalizes the limiting assumption that the total plasma density was dominated by the thermal plasma made by all previous RC–EMIC wave models, so that the RC ions were not taken into account in the real part of the wave dispersion relation [*Kozyra et al.,* 1997; *Jordanova et al.,* 1998b, 2001; *Khazanov*

et al., 2003, 2006] but only in the imaginary part, i. e., in the EMIC wave growth rate. This assumption is not always valid, especially for high L–shells during the main and recovery storm phase when the newly injected RC ions dominate the thermal plasma (see results of our simulation in Figure 1). Recent satellite observations during the November 2003 magnetic storm by *Engebretson et al.* [2007] showed that although the temperature anisotropy of energetic ($>$ 10 keV) RC protons was high during the entire 22 November 2003 perigee pass, EMIC waves were observed only in conjunction with intensification of the ion fluxes below 1 keV by over an order of magnitude. This suggests that the suprathermal plasma ($\lesssim$ 1 keV) plays an important role in the destabilization of the more energetic RC and/or plasma sheet ions such that high energy anisotropic RC and/or plasma sheet proton distributions appeared to be a necessary but not sufficient condition for occurrence of EMIC waves.

To demonstrate the role of RC ions in the real part of EMIC wave dispersion relation, we have simulated the May 1998 storm, and have presented and discussed the global distributions of the total plasma density, the energy of the He^+–mode, and the wave–induced RC precipitation. The main conclusions of our simulation can be summarized as follows.

1. The new RC ions, injected from the plasma sheet in the night MLT sector, causes plasma density enhancements for high L–shells during the main and recovery storm phases. This feature is clearly observed in our simulation (see Figure 1), and the plasma density enhancement is mostly caused by the suprathermal H^+ ($\lesssim$ 1 keV).

2. During the recovery phase, modification of the wave dispersion relation by RC

ions leads to a dramatic change in the wave patterns in the nightside MLT sector for $L > 4.75$.

3. The Cluster observations of EMIC waves and associated ion distributions during the November 2003 magnetic storm [*Engebretson et al.*, 2007] support our theoretical results presented in Figure 4. In the second row of Figure 4 we see intense EMIC waves (up to a few nT^2) in the postmidnight–dawn sector during the recovery storm phase from 82 to 84 hours. This wave activity is not observed if the RC ions are not included in the real part of the wave dispersion relation (compare the first and second rows in Figure 4).

4. The most intense wave–induced RC precipitation is due to modification of the wave dispersion relation, located in the night MLT sector. The strongest precipitating fluxes of about $8 \cdot 10^6$ $(cm^2 \cdot s \cdot sr)^{-1}$ are observed near L=5.75, MLT=2 during the early recovery phase of the storm (see hour 82 in Figure 5). The wave–induced nightside precipitation is more intense than the dayside fluxes, even if there are less intense waves (compare the results at L=4.5, MLT=16, and L=5.75, MLT=2 in the 82 hour snapshots).

Acknowledgments. This research was performed while K. Gamayunov held a NASA Postdoctoral Program appointment at NASA/MSFC. Funding in support of this study was provided by NASA grant UPN 370–16–10.

References

Akhiezer, A. I., I. A. Akhiezer, R. V. Polovin, A. G. Sitenko, and K. N. Stepanov (1975a), *Plasma Electrodynamics,* vol. 1, Pergamon, Tarrytown, N. Y.

Akhiezer, A. I., I. A. Akhiezer, R. V. Polovin, A. G. Sitenko, and K. N. Stepanov (1975b), *Plasma Electrodynamics,* vol. 2, Pergamon, Tarrytown, N. Y.

Albert, J. M. (2003), Evaluation of quasi–linear diffusion coefficients for EMIC waves in a multispecies plasma, *J. Geophys. Res., 108,* A6, 1249, doi:10.1029/2002JA009792.

Anderson, B. J., R. E. Erlandson, and L. J. Zanetti (1992a), A statistical study of Pc 1–2 magnetic pulsations in the equatorial magnetosphere: 1. Equatorial occurrence distributions, *J. Geophys. Res., 97,* 3075.

Anderson, B. J., R. E. Erlandson, and L. J. Zanetti (1992b), A statistical study of Pc 1–2 magnetic pulsations in the equatorial magnetosphere: 2. Wave properties, *J. Geophys. Res., 97,* 3089.

Anderson, B. J., and S. A. Fuselier (1994), Response of thermal ions to electromagnetic ion cyclotron waves, *J. Geophys. Res., 99,* 19413.

Angerami, J. J., and J. O. Thomas (1964), Studies of planetary atmospheres, 1, The distribution of ions and electrons in the earth's exosphere, *J. Geophys. Res., 69,* 4537.

Arnoldy, R. L., M. J. Engebretson, R. E. Denton, J. L. Posch, M. R. Lessard, N. C. Maynard, D. M. Ober, C. J. Farrugia, C. T. Russell, J. D. Scudder, R. B. Torbert, S.–H. Chen, and T. E. Moore (2005) Pc 1 waves and associated unstable

572 distributions of magnetospheric protons observed during a solar wind pressure
573 pulse, *J. Geophys. Res., 110,* A07229, doi:10.1029/2005JA011041.
574 Bezrukikh, V. V., and K. I. Gringauz (1976), The hot zone in the outer plasmasphere of
575 the Earth, *J. Atmos. Terr. Phys., 38,* 1085.
576 Bräysy, T., K. Mursula, and G. Marklund (1998), Ion cyclotron waves during a great
577 magnetic storm observed by Freja double–probe electric field instrument, *J.*
578 *Geophys. Res., 103,* 4145.
579 Chamberlain, J. W. (1963), Planetary corona and atmospheric evaporation, *Planet.*
580 *Space Sci., 11,* 901.
581 Cornwall, J. M. (1964), Cyclotron instabilities and electromagnetic emission generation
582 mechanisms, *J. Geophys. Res., 69,* 4515.
583 Cornwall, J. M. (1965), Cyclotron instabilities and electromagnetic emission in the ultra
584 low frequency and very low frequency ranges, *J. Geophys. Res., 70,* 61.
585 Cornwall, J. M., F. V. Coroniti, and R. M. Thorne (1970), Turbulent loss of ring current
586 protons, *J. Geophys. Res., 75,* 4699.
587 Cornwall, J. M., F. V. Coroniti, and R. M. Thorne (1971), Unified theory of SAR arc
588 formation at the plasmapause, *J. Geophys. Res., 76,* 4428.
589 Denton, R. E., M. K. Hudson, and I. Roth (1992), Loss–cone–driven ion cyclotron waves
590 in the magnetosphere, *J. Geophys. Res., 97,* 12093.
591 Engebretson, M. J., A. Keiling, K.–H. Fornacon, C. A. Cattell, J. R. Johnson, J. L.
592 Posch, S. R. Quick, K.–H. Glassmeier, G. K. Parks, and H. Réme (2007), Cluster
593 observations of Pc 1–2 waves and associated ion distributions during the October

and November 2003 magnetic storms, *Planet. Space Sci., 55,* 6, 829.

Engebretson, M. J., W. K. Peterson, J. L. Posch, M. R. Klatt, B. J. Anderson, C. T. Russell, H. J. Singer, R. L. Arnoldy, H. Fukunishi (2002), Observations of two types of Pc 1–2 pulsations in the outer dayside magnetosphere, *J. Geophys. Res., 107,* A12, 1451, doi:10.1029/2001JA000198.

Engebretson, M. J., J. L. Posch, M. R. Lessard, R. L. Arnoldy, D. E. Rowland, S.–H. Chen, T. E. Moore, W. K. Peterson, T. G. Onsager, J. R. Johnson, and C. T. Russell (2005), Pc 1 waves and associated unstable distributions of magnetospheric protons during three extended conjunctions between the Polar satellite and Antarctic ground stations, *IAGA Meeting,* Toulouse, France, July 25, 2005.

Erlandson, R. E., and A. J. Ukhorskiy (2001), Observations of electromagnetic ion cyclotron waves during geomagnetic storms: Wave occurrence and pitch angle scattering, *J. Geophys. Res., 106,* 3883.

Erlandson, R. E., L. J. Zanetti, T. A. Potemra, L. P. Block, and G. Holmgren (1990), Viking magnetic and electric field observations of Pc 1 waves at high latitudes, *J. Geophys. Res., 95,* 5941.

Farrugia, C. J., V. K. Jordanova, M. P. Freeman, C. C. Cocheci, R. L. Arnoldy, M. Engebretson, P. Stauning, G. Rostoker, M. F. Thomsen, G. D. Reeves, and K. Yumoto (2003), Large-scale geomagnetic effects of May 4, 1998, *Adv. Space Res., 31/4,* 1111.

Foat, J. E., R. P. Lin, D. M. Smith, F. Fenrich, R. Millan, I. Roth, K. R. Lorentzen,

616 M. P. McCarthy, G. K. Parks, and J. P. Treilhou (1998), First detection of a
617 terrestrial MeV X–ray burst, *Geophys. Res. Lett., 25,* 4109.
618 Fok, M.–C., J. U. Kozyra, A. F. Nagy, C. E. Rasmussen, and G. V. Khazanov (1993),
619 A decay model of equatorial ring current and the associated aeronomical
620 consequences, *J. Geophys. Res., 98,* 19381.
621 Fraser, B. J., and T. S. Nguyen (2001), Is the plasmapause a preferred source region of
622 electromagnetic ion cyclotron waves in the magnetosphere?, *J. Atmos. Sol. Terr.*
623 *Phys., 63,* 1225.
624 Fuselier, S. A., and B. J. Anderson (1996) Low–energy He^+ and H^+ distributions and
625 proton cyclotron waves in the afternoon equatorial magnetosphere, *J. Geophys.*
626 *Res., 101,* 13255.
627 Galeev, A. A. (1975), Plasma turbulence in the magnetosphere with special regard to
628 plasma heating, in *Physics of the Hot Plasma in the Magnetosphere,* edited by B.
629 Hultquist, and L. Stenflo, p. 251, Plenum Press, N. Y.–London.
630 Garcia, H. A., and W. N. Spjeldvik (1985), Anisotropy characteristics of geomagnetically
631 trapped ions, *J. Geophys. Res., 90,* 347.
632 Gendrin, R., M. Ashour–Abdalla, Y. Omura, and K. Quest (1984), Linear analysis of
633 ion–cyclotron interaction in a multicomponent plasma, *J. Geophys. Res., 89,*
634 9119.
635 Gomberoff, L., and R. Neira (1983), Convective growth rate of ion cyclotron waves in a
636 $H^+ - He^+$ and $H^+ - He^+ - O^+$ plasma, *J. Geophys. Res., 88,* 2170.
637 Gonzalez, W. D., B. T. Tsurutani, A. L. C. Gonzalez, E. J. Smith, F. Tang, and S.–I.

638 Akasofu (1989), Solar wind–magnetosphere coupling during intense magnetic
639 storms (1978–1979), *J. Geophys. Res., 94,* 8835.

640 Gorbachev, O. A., G. V. Khazanov, K. V. Gamayunov, and E. N. Krivorutsky (1992), A
641 theoretical model for the ring current interaction with the Earth's plasmasphere,
642 *Planet. Space Sci., 40,* 859.

643 Gringauz, K. I. (1983), Plasmasphere and its interaction with ring current, *Space Sci.*
644 *Rev., 34,* 245.

645 Gringauz, K. I. (1985), Structure and properties of the Earth plasmasphere, *Adv. Space*
646 *Res., 5,* 391.

647 Gurgiolo, C., B. R. Sandel, J. D. Perez, D. G. Mitchell, C. J. Pollock, and B. A. Larsen
648 (2005), Overlap of the plasmasphere and ring current: Relation to subauroral
649 ionospheric heating, *J. Geophys. Res., 110,* A12217, doi:10.1029/2004JA010986.

650 Horne, R. B., and R. M. Thorne (1993), On the preferred source location for the
651 convective amplification of ion cyclotron waves, *J. Geophys. Res., 98,* 9233.

652 Horne, R. B., and R. M. Thorne (1997), Wave heating of He^+ by electromagnetic ion
653 cyclotron waves in the magnetosphere: Heating near $H^+ - He^+$ bi–ion resonance
654 frequency, *J. Geophys. Res., 102,* 11457.

655 Horwitz, J. L., C. R. Baugher, C. R. Chappell, E. G. Shelley, D. T. Young, and R.
656 R. Anderson (1981), ISEE 1 observations of thermal plasma during periods of
657 quieting magnetic activity, *J. Geophys. Res., 86,* 9989.

658 Iyemori, T., and K. Hayashi (1989), Pc 1 micropulsations observed by Magsat in
659 ionospheric F region, *J. Geophys. Res., 94,* 93.

660 Jordanova, V. K., C. J. Farrugia, L. Janoo, J. M. Quinn, R. B. Torbert, K. W. Ogilvie,
661 R. P. Lepping, J. T. Steinberg, D. J. McComas, and R. D. Belian (1998a),
662 October 1995 magnetic cloud and accompanying storm activity: Ring current
663 evolution, *J. Geophys. Res., 103,* 79.
664 Jordanova, V. K., C. J. Farrugia, J. M. Quinn, R. M. Thorne, K. W. Ogilvie, R. P.
665 Lepping, G. Lu, A. J. Lazarus, M. F. Thomsen, and R. D. Belian (1998b), Effect
666 of wave-particle interactions on ring current evolution for January 10–11, 1997:
667 Initial results, *Geophys. Res. Lett., 25,* 2971.
668 Jordanova, V. K., C. J. Farrugia, R. M. Thorne, G. V. Khazanov, G. D. Reeves, and
669 M. F. Thomsen, Modeling ring current proton precipitation by EMIC waves
670 during the May 14–16, 1997, storm, *J. Geophys. Res., 106,* 7, 2001.
671 Jordanova, V. K., L. M. Kistler, J. U. Kozyra, G. V. Khazanov, and A. F. Nagy (1996),
672 Collisional losses of ring current ions, *J. Geophys. Res., 101,* 111.
673 Jordanova, V. K., J. U. Kozyra, G. V. Khazanov, A. F. Nagy, C. E. Rasmussen, and
674 M.–C. Fok (1994), A bounce–averaged kinetic model of the ring current ion
675 population, *Geophys. Res. Lett., 21,* 2785.
676 Jordanova, V. K., J. U. Kozyra, A. F. Nagy, and G. V. Khazanov (1997), Kinetic model
677 of the ring current–atmosphere interactions, *J. Geophys. Res., 102,* 14279.
678 Kennel, C. F., and H. E. Petschek (1966), Limit on stably trapped particle fluxes, *J.*
679 *Geophys. Res., 71,* 1.
680 Khazanov, G. V., K. V. Gamayunov, D. L. Gallagher, and J. U. Kozyra (2006), Self–
681 consistent model of magnetospheric ring current and propagating electromagnetic

682 ion cyclotron waves: Waves in multi ion magnetosphere, *J. Geophys. Res., 111,*
683 A10202, doi:10.1029/2006JA011833.
684 Khazanov, G. V., K. V. Gamayunov, D. L. Gallagher, J. U. Kozyra, and M. W. Liemohn
685 (2007), Self–consistent model of magnetospheric ring current and propagating
686 electromagnetic ion cyclotron waves. 2. Wave induced ring current precipitation
687 and thermal electron heating, *J. Geophys. Res.,* in press.
688 Khazanov, G. V., K. V. Gamayunov, and V. K. Jordanova, Self–consistent model
689 of magnetospheric ring current ions and electromagnetic ion cyclotron
690 waves: The 2–7 May 1998 storm (2003), *J. Geophys. Res., 108,* A12, 1419,
691 doi:10.1029/2003JA009856.
692 Khazanov, G. V., K. V. Gamayunov, V. K. Jordanova, and E. N. Krivorutsky (2002), A
693 self–consistent model of the interacting ring current ions and electromagnetic ion
694 cyclotron waves, initial results: Waves and precipitating fluxes, *J. Geophys. Res.,*
695 *107,* A6, 1085, doi:10.1029/2001JA000180.
696 Kozyra, J. U., T. E. Cravens, A. F. Nagy, E. G. Fontheim, and R. S. B. Ong (1984),
697 Effects of energetic heavy ions on electromagnetic ion cyclotron wave generation
698 in the plasmapause region, *J. Geophys. Res., 89,* 2217.
699 Kozyra, J. U., V. K. Jordanova, R. B. Horne, and R. M. Thorne (1997), Modeling of the
700 contribution of Electromagnetic Ion Cyclotron (EMIC) waves to stromtime ring
701 current erosion, in *Magnetic Storms, Geophys. Monogr. Ser.,* vol. 98, edited by
702 B. T. Tsurutani, W. D. Gonzalez, Y. Kamide, and J. K. Arballo, p. 187, AGU,
703 Washington, D. C..

LaBelle, J., R. A. Treumann, W. Baumjohann, G. Haerendel, N. Sckopke, G. Paschmann, and H. Lühr (1988), The duskside plasmapause/ring current interface: Convection and plasma wave observations, *J. Geophys. Res., 93,* 2573.

Lorentzen, K. R., M. P. McCarthy, G. K. Parks, J. E. Foat, R. M. Millan, D. M. Smith, R. P. Lin, and J. P. Treilhou (2000), Precipitation of relativistic electrons by interaction with electromagnetic ion cyclotron waves, *J. Geophys. Res., 105,* 5381.

Loto'aniu, T. M., B. J. Fraser, and C. L. Waters (2005), Propagation of electromagnetic ion cyclotron wave energy in the magnetosphere, *J. Geophys. Res., 110,* A07214, doi:10.1029/2004JA010816.

Loto'aniu, T. M., R. M. Thorne, B. J. Fraser, and D. Summers (2006), Estimating relativistic electron pitch angle scattering rate using properties of the electromagnetic ion cyclotron wave spectrum, *J. Geophys. Res., 111,* A04220, doi:10.1029/2005JA011452.

Lyons, L. R., and R. M. Thorne (1972), Parasitic pitch angle diffusion of radiation belt particles by ion cyclotron waves *J. Geophys. Res., 77,* 5608.

Lyons, L. R., and D. J. Williams (1984), *Quantitative Aspects of Magnetospheric Physics,* D. Reidel, Dordrecht.

Mauk, B. H. (1982), Helium resonance and dispersion effects on geostationary Alfvén/ion cyclotron waves, *J. Geophys. Res., 87,* 9107.

Meredith, N. P., R. M. Thorne, R. B. Horne, D. Summers, B. J. Fraser, and R. R. Anderson (2003), Statistical analysis of relativistic electron energies for cyclotron

726 resonance with EMIC waves observed on CRRES, *J. Geophys. Res., 108,* A6,
727 1250, doi:10.1029/2002JA009700.
728 Rairden, R. L., L. A. Frank, and J. D. Craven (1986), Geocoronal imaging with
729 Dynamics Explorer, *J. Geophys. Res., 91,* 13613.
730 Rasmussen, C. E., S. M. Guiter, and S. G. Thomas (1993), Two–dimensional model of
731 the plasmasphere: Refilling time constants, *Planet. Space Sci., 41,* 35.
732 Rauch, J. L., and A. Roux (1982), Ray tracing of ULF waves in a multicomponent
733 magnetospheric plasma: Consequences for the general mechanism of Ion
734 Cyclotron Waves, *J. Geophys. Res., 87,* 8191.
735 Roux, A., S. Perraut, J. L. Rouch, C. de Villedary, G. Kremser, A. Korth, and D. T.
736 Young (1982), Wave–particle interactions near Ω_{He^+} observed on board GEOS 1
737 and 2: 2. Generation of ion cyclotron waves and heating of He^+ ions, *J. Geophys.*
738 *Res., 87,* 8174.
739 Sheldon, R. B., and D. C. Hamilton (1993), Ion transport and loss in the Earth's quiet
740 ring current, 1, Data and standard model, *J. Geophys. Res., 98,* 13491.
741 Soraas, F., K. Aarsnes, J. A. Lundblad, and D. S. Evans (1999), Enhanced pitch angle
742 scattering of protons at mid–latitudes during geomagnetic storms, *Phys. Chem.*
743 *Earth (C), 24,* 287.
744 Stern, D. P. (1975), The motion of a proton in the equatorial magnetosphere, *J.*
745 *Geophys. Res., 80,* 595.
746 Stix, T. H. (1992), *Waves in Plasmas,* Am. Inst. of Phys., College Park, Md.
747 Summers, D., and R. M. Thorne (2003), Relativistic electron pitch–angle scattering

748 by electromagnetic ion cyclotron waves during geomagnetic storms, *J. Geophys.*
749 *Res., 108,* A4, doi:10.1029/2002JA009489.
750 Thorne, R., and R. Horne (1994), Energy transfer between energetic ring current H^+
751 and O^+ by electromagnetic ion cyclotron waves, *J. Geophys. Res., 99,* 17275.
752 Thorne, R., and R. Horne (1997), Modulation of electromagnetic ion cyclotron instability
753 due to interaction with ring current O^+ during the geomagnetic storms, *J.*
754 *Geophys. Res., 102,* 14155.
755 Thorne, R. M., and C. F. Kennel (1971), Relativistic electron precipitation during
756 magnetic storm main phase, *J. Geophys. Res., 76,* 4446.
757 Volland, H. (1973), A semiempirical model of large–scale magnetospheric electric fields,
758 *J. Geophys. Res., 78,* 171.
759 Walt, M., and H. D. Voss (2001), Losses of ring current ions by strong pitch angle
760 scattering, *Geophys. Res. Lett., 28,* 3839.
761 Walt, M., and H. D. Voss (2004), Proton precipitation during magnetic storms
762 in August through November 1998, *J. Geophys. Res., 108,* A02201,
763 doi:10.1029/2003JA010083.
764 Yahnina, T. A., A. G. Yahnin, J. Kangas, J. Manninen, D. S. Evans, A. G. Demekhov,
765 V. Yu. Trakhtengerts, M. F. Thomsen, G. D. Reeves, and B. B. Gvozdevsky
766 (2003), Energetic particle counterparts for geomagnetic pulsations of Pc 1 and
767 IPDP types, *Annales Geophysicae, 21,* 2281.
768 Young, D. T. (1983), Heavy ion plasmas in the outer magnetosphere, *J. Geophys. Res.,*
769 *52,* 167.

770 Young, D. T., H. Balsiger, and J. Geiss (1982), Correlations of magnetospheric ion
771 composition with geomagnetic and solar activity, *J. Geophys. Res., 87,* 9077.
772 Young D. T., T. J. Geiss, H. Balsiger, P. Eberhardt, A. Ghiedmetti, and H. Rosenbauer
773 (1977), Discovery of He^{2+} and O^{2+} ions of terrestrial origin in the outer
774 magnetosphere, *Geophys. Res. Lett., 4,* 561.
775 Young D. T., S. Perraut, A. Roux, C. de Villedary, R. Gendrin, A. Korth, G. Kremser,
776 and D. Jones (1981), Wave–particle interactions near Ω_{He^+} observed on GEOS 1
777 and 2: 1. Propagations of ion cyclotron waves in He^+–rich plasma, *J. Geophys.*
778 *Res., 86,* 6755.
779 Zaharia, S., V. K. Jordanova, M. F. Thomsen, and G. D. Reeves (2006), Self–
780 consistent modeling of magnetic fields and plasmas in the inner magneto-
781 sphere: Applicationto a geomagnetic storm, *J. Geophys. Res., 111,* A11S14,
782 doi:10.1029/2006JA011619.

783 K. V. Gamayunov, National Space Science and Technology Center, NASA Marshall
784 Space Flight Center, Space Science Department, 320 Sparkman Drive, Huntsville, AL
785 35805, USA. (e–mail: konstantin.gamayunov@msfc.nasa.gov)
786 G. V. Khazanov, National Space Science and Technology Center, NASA Marshall
787 Space Flight Center, Space Science Department, 320 Sparkman Drive, Huntsville, AL
788 35805, USA. (e–mail: george.khazanov@msfc.nasa.gov)

789 Received _____

Figure 1. Equatorial plasma density distributions during the May 1998 event. The first row shows the cold electron plasma density distribution from the *Rasmussen et al.* [1993] model, and the second row provides a sum of cold plasma density and RC H^+ density as it follows from the simulation. The first, the second, and the third plasma sheet ion injections affect the total density distribution during 33–48, 58–68, and 78–90 hours, respectively. The specified hours are counted from 0000 UT on 1 May, 1998.

Figure 2. Simulated phase space distribution function for the RC H^+. All the PSDFs are shown in the equatorial plane, and integrated over the entire solid angle. For each PSDFs, the first and the second numbers in parenthesis are the L–shell and MLT location, respectively. The corresponding RC proton temperature along the geomagnetic field line, $T_{\|}$, is calculated for the entire energy range. Note that there are the linear and logarithmic energy scales in the left–hand and right–hand boxes, respectively.

Figure 3. Equatorial growth/damping rates versus the wave normal angle for the He^+–mode of EMIC waves. The RC is assumed to be entirely made up of energetic protons, the thermal plasma consists of the cold electrons, and 77% of H^+, 20% of He^+, and 3% of O^+, and the wave resonate interaction with thermal plasma is omitted. All the results are obtained for the wave frequency $\nu = \omega/2\pi = 0.475$ Hz, and taken from our global model at location L=5.25, MLT=15 ($B = 215.3$ nT), at 48 hours after 1 May 1998, 0000 UT. (a) The electron number density is also determined by the global model, and $n_e = n_0 = 68.3$ cm^{-3} (nominal case). In order to produce the results (b), (c), and (d), we keep all parameters the same, except the electron number densities $n_e = 1.2 \times n_0$, $n_e = 1.5 \times n_0$, and $n_e = 2 \times n_0$ are respectively adopted.

Figure 4. Snapshots of the equatorial (MLT, L–shell) distributions of squared wave magnetic field for the He^+–mode. The results are obtained by solving equations (1) and (2) along with the ray tracing equations. The first row corresponds to the case when the RC ions are only treated as a source of free energy to generate waves, and omitted in
793 the real part of the wave dispersion relation. The second row demonstrates distribution when the RC ions are taken into account in both the real and imaginary parts of the wave dispersion relation. In both cases, the total ion composition is assumed to be 77% of H^+, 20% of He^+, and 3% of O^+ through an entire simulation domain.

Figure 5. The RC proton precipitating fluxes averaged over the equatorial pitch–angle loss cone and integrated over the energy range $1 - 50$ keV. The first row represents the
794 results without the RC ions in the real part of the EMIC wave dispersion relation. The second row shows precipitation in a case when the RC ions are taken into account in both the real and imaginary parts of the wave dispersion relation.

May 2–7, 1998: Thermal and
Sum of Thermal and RC Plasma Densities
N [cm ⁻³]
10¹
10²
hr 33
hr 34
hr 60
hr 78
hr 80
hr 82
hr 84
6
12
0
18
2
4
6

Figure 1.

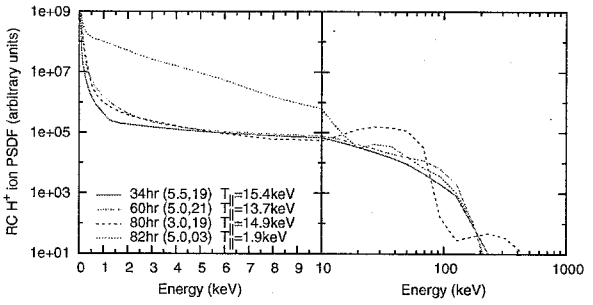

799

800 **Figure 2.**

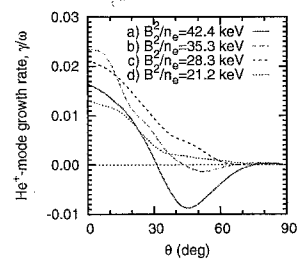

801

802 **Figure 3.**

May 2–7, 1998: B–field Spectrogram (W/Ray)
Without and With RC Ions in Dispersion Relation
Bw² [nT²]
10⁻² 10⁻¹ 10⁰ 10¹
hr 33
hr 34
hr 60
hr 78
hr 80
hr 82
hr 84
6
12
0
18
2 4 6

Figure 4.

May 2–7, 1998: 1 – 50 keV Ion Fluxes (W/Kay)
Without and With RC Ions in Dispersion Relation
[1/cm²/s/sr]
10¹ 10² 10³ 10⁴ 10⁵ 10⁶
hr 33
hr 34
hr 60
hr 78
hr 80
hr 82
hr 84
ΔR
6
12
0
18
2
4
6

Figure 5.